


RESEARCH ARTICLE

Extracellular vesicles from adipose tissue-derived stem cells alleviate osteoporosis through osteoprotegerin and *miR-21-5p*

Kyoung Soo Lee^{1,2}  | Jeongmi Lee³  | Hark Kyun Kim³  | Seung Ho Yeom²  |
 Chang Hee Woo²  | Youn Jae Jung²  | Ye Eun Yun¹  | So Young Park²  |
 Jihoon Han³  | Eunae Kim³  | Jae Hoon Sul³  | Jae Min Jung⁴  |
 Jae Hyung Park^{2,4,5,6}  | Ji Suk Choi²  | Yong Woo Cho^{1,2}  | Dong-Gyu Jo^{2,3,5,6} 

¹ Department of Materials Science and Chemical Engineering, Hanyang University ERICA, Ansan, Korea

² Exostemtech, Inc., Ansan, Korea

³ School of Pharmacy, Sungkyunkwan University, Suwon, Korea

⁴ School of Chemical Engineering, College of Engineering, Sungkyunkwan University, Suwon, Korea

⁵ Biomedical Institute for Convergence, Sungkyunkwan University, Suwon, Korea

⁶ Department of Health Science and Technology, SAIHST, Sungkyunkwan University, Seoul, Korea

Correspondence

Dong-Gyu Jo, School of Pharmacy, Sungkyunkwan University, Suwon, Korea.

Email: jodg@skku.edu

Ji Suk Choi, Exostemtech, Inc., Ansan, Korea.

Email: jschoi@exostemtech.com

Yong Woo Cho, Department of Materials Science and Chemical Engineering, Hanyang University ERICA, Ansan, Korea.

Email: ywcho7@hanyang.ac.kr

Kyoung Soo Lee and Jeongmi Lee contributed equally to this work and are joint first authors.

Funding information

National Research Foundation, Grant/Award Numbers: NRF-2018M3A9H1023767, NRF-2019R1A5A2027340, NRF-2019R1A2C3011422; Ministry of Food and Drug Safety, Grant/Award Number: 18172MFDS173; Ministry of Oceans and Fisheries' R&D project, Korea, Grant/Award Number: 1525011845; Ministry of Education, Grant/Award Number: 2020R1A6C101A191; Ministry of SMEs and Startups, MSS

Abstract

Osteoporosis is one of the most common skeletal disorders caused by the imbalance between bone formation and resorption, resulting in quantitative loss of bone tissue. Since stem cell-derived extracellular vesicles (EVs) are growing attention as novel cell-free therapeutics that have advantages over parental stem cells, the therapeutic effects of EVs from adipose tissue-derived stem cells (ASC-EVs) on osteoporosis pathogenesis were investigated. ASC-EVs were isolated by a multi-filtration system based on the tangential flow filtration (TFF) system and characterized using transmission electron microscopy, dynamic light scattering, zeta potential, flow cytometry, cytokine arrays, and enzyme-linked immunosorbent assay. EVs are rich in growth factors and cytokines related to bone metabolism and mesenchymal stem cell (MSC) migration. In particular, osteoprotegerin (OPG), a natural inhibitor of receptor activator of nuclear factor- κ B ligand (RANKL), was highly enriched in ASC-EVs. We found that the intravenous administration of ASC-EVs attenuated bone loss in osteoporosis mice. Also, ASC-EVs significantly inhibited osteoclast differentiation of macrophages and promoted the migration of bone marrow-derived MSCs (BM-MSCs). However, OPG-depleted ASC-EVs did not show anti-osteoclastogenesis effects, demonstrating that OPG is critical for the therapeutic effects of ASC-EVs. Additionally, small RNA sequencing data were analysed to identify miRNA candidates related to anti-osteoporosis effects. *miR-21-5p* in ASC-EVs inhibited osteoclast differentiation through *Acvr2a* down-regulation. Also, *let-7b-5p* in ASC-EVs significantly reduced the expression of genes related to osteoclastogenesis. Finally, ASC-EVs reached the bone tissue after they were injected intravenously, and they remained longer. OPG, *miR-21-5p*, and *let-7b-5p* in ASC-EVs inhibit osteoclast differentiation and reduce gene expression related to bone resorption, suggesting that ASC-EVs are highly promising as cell-free therapeutic agents for osteoporosis treatment.

KEYWORDS

extracellular vesicles, human adipose tissue-derived stem cells, let-7b-5p, miR-21-5p, osteoporosis, osteoprotegerin

This is an open access article under the terms of the [Creative Commons Attribution-NonCommercial License](https://creativecommons.org/licenses/by-nc/4.0/), which permits use, distribution and reproduction in any medium, provided the original work is properly cited and is not used for commercial purposes.

© 2021 The Authors. *Journal of Extracellular Vesicles* published by Wiley Periodicals, LLC on behalf of the International Society for Extracellular Vesicles

1 | INTRODUCTION

Osteoporosis is a systemic bone disease characterized by low bone mass and microstructural changes, leading to reduced bone strength and increased risk of fracture. The pathogenesis of osteoporosis is the imbalance between bone formation and resorption caused by various risk factors, such as ageing, endocrine, metabolic and nutritional disorders, and some medications (J. T. Lin & Lane, 2004).

Most current agents are bone resorption inhibitors for osteoporosis treatment, including bisphosphonates, oestrogen, and selective oestrogen receptor modulators (Saita et al., 2015). These antiresorptive agents increase bone mineral density (BMD) and reduce the risk of osteoporosis fractures. However, long-term safety and efficacy are ongoing concerns (Khosla & Hofbauer, 2017; Lo et al., 2010).

Mesenchymal stem cells (MSCs) provide a promising cell source for clinical applications in osteoporosis treatment (Cho et al., 2012; Ocarino et al., 2010; Z. Wang et al., 2006). MSC transplantation may improve bone quality by homing to a damaged bone and differentiating into osteoblasts or secreting various factors related to bone repair (Antebi et al., 2014; Yao et al., 2013). Despite MSC's therapeutic potential for osteoporosis, there are some hurdles, such as cell entrapment in non-target organs, low survival, and uncertainty of stem cell fate after transplantation (Ocarino et al., 2010; Tolar et al., 2007).

Many studies have recently reported that MSCs participate in tissue regeneration via the secretion of paracrine factors rather than direct action at injured tissues (Biancone et al., 2012; Caplan & Dennis, 2006; Phinney & Pittenger, 2017). Extracellular vesicles (EVs) are small secretory vesicles involved in the paracrine effects of MSCs. EVs contain cytosolic proteins, lipids, and genetic factors, such as mRNA, miRNA, and ncRNA, for intercellular communication and cell differentiation (Jung et al., 2020; Qi et al., 2016; Vlassov et al., 2012). Also, they have therapeutic functions like those of their parent stem cells, such as tissue repair and immunomodulation (Bruno et al., 2015; Woo et al., 2020). MSC EVs can be applied as promising tools to overcome the limitations of stem cell therapy regarding efficacy and safety concerns as well as administration and management (Lener et al., 2015). Several studies have shown that MSC EVs induce bone regeneration in diverse *in vivo* bone defect models (Furuta et al., 2016; Qi et al., 2016; Qin et al., 2016; Zhang et al., 2016). Human adipose tissue-derived stem cells (hASCs) are MSCs abundant in adipose tissue. ASCs have been widely used as a source of EV production because of their plentifulness and accessibility compared with bone marrow-derived MSCs (BM-MSCs), while it has a similar ability to differentiate into mesodermal lineage cells (Gimble et al., 2007; Maqsood et al., 2020). Treatments based on EVs from adipose tissue-derived stem cells (ASC-EVs) have been investigated in tissue repair and disease models (Liu & Holmes, 2021). Two studies reported that ASC-EVs increased the osteogenic differentiation and bone formation in the calvarial defect model (S. Chen, Tang, et al. 2019; W. Li et al., 2018). However, the effects of ASC-EVs on the osteoporosis model remain unknown.

Osteoclasts located on the bone surface play a significant role in bone resorption. Receptor activator of nuclear factor- κ B ligand (RANKL) induces osteoclast differentiation by binding to RANK, and activated osteoclasts secrete proteolytic enzymes and acids (Tobeiha et al., 2020). Osteoprotegerin (OPG) is a decoy receptor for RANKL that inhibits osteoclast differentiation by blocking RANKL-RANK interaction. Disruptions in the OPG to RANKL ratio occur in bone resorption disorders, such as oestrogen deficiency and hyperparathyroidism (M. McClung, 2007). Thus, the RANK-RANKL-OPG pathway is critical for regulating the balance between bone formation and resorption.

In this study, the therapeutic effects of EVs secreted from ASC-EVs on ovariectomy (OVX)-induced osteoporosis animal model were investigated. ASC-EVs significantly contributed to the inhibition of osteoclast differentiation and the promotion of bone healing in osteoporotic mice by delivering various bone regulatory proteins. Whether these therapeutic effects are dependent on OPG was determined, and miRNA candidates for regulating bone resorption were found. Therefore, ASC-EV is highly promising as a cell-free therapeutic agent for osteoporosis treatment.

2 | MATERIALS AND METHODS

2.1 | Cell culture and collection of conditioned media

ASCs were purchased from CEFO Bio Co., Ltd. (Seoul, Korea) and cultured in Dulbecco's Modified Eagle's Medium (DMEM) supplemented with 10% foetal bovine serum (FBS) and 1% penicillin/streptomycin (P/S) at 37°C in humidified air containing 5% CO₂. ASCs were cultured and maintained to reach 90% confluence at passage 5. Cells were washed with phosphate-buffered saline (PBS), and the medium was replaced with serum-free DMEM for 24 h to collect conditioned medium (CM). Collected CM (500 ml) was centrifuged at 300 × *g* for 10 min to remove cell debris, and the supernatant was filtered using a 0.22 μm bottle top filter to eliminate macrovesicles.

2.2 | Extracellular vesicles isolation and characterization

EVs were isolated from CM (500 ml) by a multi-filtration system based on tangential flow filtration (TFF) (Minimate TFF System; Pall Corporation, Port Washington, NY, USA), based on previous protocols (Woo et al., 2020). The CM was subjected to TFF with a 300 kDa MWCO capsule (Minimate TFF Capsule; Pall Corporation, Port Washington, NY, USA). Continuous circulation was performed at a feed rate of 30~60 ml/min, and the filtrate rate was controlled around 4 ml/min to remove the contaminants below 300 kDa. Subsequently, two more TFF cycle was performed by adding 50 ml of PBS to wash residual contaminants in concentrated EV solution. Throughout the TFF process, the pressure was controlled not to exceed 1 bar at room temperature. EVs were obtained in a final volume of approximately 10 ml. EVs were stored in a freezer at -70°C until use. EVs were quantified using a micro-bicinchoninic acid protein assay (Thermo Scientific, Rockford, IL, USA) and nanoparticle tracking analysis (LM-10; Malvern Instruments Ltd., Worcestershire, UK) equipped with a 642 nm laser module. EVs were diluted in PBS to obtain a concentration within the recommended measurement range (20–30 particles/frame), corresponding to dilutions from 1:10 to 1:100 depending on the initial sample concentration. The software settings for analysis were as follows: detection threshold, 3; temperature, between 20°C and 25°C ; the number of frames, 30; and measurement time, 30 s.

2.3 | Transmission electron microscopy

EVs were fixed with 1% glutaraldehyde solution for 5 min and washed with distilled water thrice. The fixed EVs were centrifuged at $13,000 \times g$ for 3 min, based on previous protocols (Jung et al., 2020). Then, the supernatant was removed. Next, the samples were dehydrated in absolute ethanol for 10 min and placed on formvar-carbon-coated copper grids (TED PELLA, Inc., Redding, CA, USA). The grids were contrasted with 1% phosphotungstic acid for 1 min and then washed with distilled water thrice. The grids were dried off completely and then examined with a JEM-2100F field-emission electron microscope (JEOL Ltd., Japan). For cryo-TEM, an aliquot of concentrated EVs was applied to the Lacey carbon grid (Electron Microscopy Science, Hatfield, PA, USA). The grids were stored in liquid nitrogen, transferred to a cryo-specimen holder, and maintained at -180°C . Images were collected at a magnification of $\times 18,000$ to $\times 29,000$ on the Tecnai F20 Twin TEM operated at 200 kV.

2.4 | Flow cytometry analysis

Flow cytometry analysis (FACS) of EVs was performed using a commercially available ExoStep (Immunostep, Salamanca, Spain) according to the manufacturer's protocol. Briefly, EVs were captured on $6.5 \mu\text{m}$ microbeads with anti-CD63 capture antibodies provided in the kit. The EVs-microbead complexes were incubated with anti-CD9 (Immunostep), anti-CD63 (Immunostep), anti-CD81 (Immunostep), anti-GM130 (Novus Biologicals, Colorado, USA), and anti-calnexin (Novus Biologicals) at 4°C for 1 h and stained by streptavidin-phycoerythrin (PE). Mouse IgG1 antibody (Bio-Rad, Hercules, CA, USA) was used as an isotype control. Samples were analysed by FACS (Novocyte Flow Cytometer; ACEA Bioscience, Inc., San Diego, CA, USA). Data acquisition and analysis were performed using NovoExpress software.

2.5 | Ovariectomized mouse models

Eight-week-old female ICR (CD-1) mice were purchased from Japan SLC, Inc., and 24 mice were bilaterally OVX while six mice underwent the sham operation. All animal experiments were performed with approval from the Institutional Review Board of Hanyang University. Three weeks after OVX, mice were randomly divided into four groups ($n = 6$) and intravenously injected with ASC-EVs (1×10^8 or 5×10^8 particles/ $100 \mu\text{l}$ PBS, thrice a week for 2 weeks), hASCs (5×10^5 cells/ $100 \mu\text{l}$ PBS, once a week for 2 weeks) (Cho et al., 2012), or an equal volume of PBS, respectively. At 5 weeks after injection, mice were sacrificed, and the left femurs of each group were harvested. The specimens were fixed in 4% paraformaldehyde for 2 days and subsequently scanned using micro-computed tomography (μCT ; Bruker, Kontich, Belgium) at $6.75 \mu\text{m}$ resolution. Three-dimensional (3D) images were generated using the CTvox program (Bruker, Billerica, MA, USA).

2.6 | Migration assay

The migration of human bone marrow MSCs (BM-MSCs, CEFO CO., Ltd, Seoul, Korea) was assessed using transwell with $8 \mu\text{m}$ pores (Corning, Corning, NY, USA). Briefly, serum-starved BM-MSCs were seeded at 5×10^4 cells in $100 \mu\text{l}$ in DMEM supplemented with 2% FBS and 1% penicillin-streptomycin (P/S) onto the upper chamber. EVs (1×10^8 , 5×10^8 , or 10×10^8 particles/ml

EVs) and vehicle control (PBS) were added to the lower chambers. Cells were incubated for 18 h at 37°C, and non-migrated cells were removed from the inserts using cotton swabs. Migrated cells at the bottom of the membrane were fixed with 4% paraformaldehyde for 10 min. Cells were subsequently stained with 0.05% crystal violet staining solution for 15 min. After the inserts were completely dried, stained cells were visualized with a light microscope, and the stained areas were quantified using ImageJ software.

2.7 | Osteoclastogenesis inhibition test

RAW264.7 cells were seeded at 1×10^4 cells into 48-well plates and incubated for 4 days in osteoclast differentiation medium (DMEM containing 3% heat-inactivated FBS, 1% P/S, and 20 ng/ml RANKL) supplemented with PBS, OPG (0.5 and 50 ng/ml), or ASC-EVs (1×10^8 , 5×10^8 , or 10×10^8 particles/ml), respectively. The medium was changed every 2 days. On day 4, cells were incubated in the tartrate-resistant acid phosphate (TRAP) staining solution (Kamiya Biomedical Company, Seattle, WA, USA) for 3 h. Absorbance readings were then taken at 540 nm using a microplate spectrophotometer. On day 6 of differentiation, cells were washed with PBS and fixed with 4% paraformaldehyde solution for 10 min. Cells were stained with a TRAP staining kit according to the manufacturer's recommended protocol. The stained cells were photographed with a light microscope equipped with a CCD camera, and multinucleated TRAP-positive osteoclasts (more than three nuclei) were counted.

2.8 | Small RNA sequencing

RNA isolation from ASC-EVs, library generation, cluster amplification, and sequencing were performed by Macrogen (Seoul, Korea). Samples for small RNA sequencing were prepared as described previously (Jung et al., 2020). Briefly, RNA was extracted from ASC-EVs using the Maxwell RSC miRNA from plasma (Promega). Libraries were then generated using the SMARTer smRNA-seq Kit for Illumina (Takara Bio, Shiga, Japan) according to the manufacturer's protocol. The Illumina HiSeq 2500 instrument (Illumina, San Diego, CA, USA) was used for sequencing the libraries. Target genes of each miRNA in ASC-EVs were predicted using publicly available algorithms, including TargetScan 7.2 (<http://www.targetscan.org>) and miRDB (www.mirdb.org).

2.9 | Extracellular vesicles labelling and cellular uptake assay

EVs were labelled with PKH67 (Sigma, St. Louis, MO, USA) for 30 s at room temperature. The labelled EV suspension was filtered with an Exosome Spin Column (MWCO 3000 Da; Invitrogen, CA, USA) to remove the unbound-free dye. Murine macrophage RAW264.7 cells (1×10^5) were seeded in a six-well confocal dish (SPL Life Sciences, Korea) and incubated at 37°C with 1×10^9 particles/ml PKH67-labeled EVs for 12 h. Nuclei were stained with 4',6-diamidino-2-phenylindole (DAPI), and cells were observed under confocal laser scanning microscopy (Zeiss, Weimar, Germany).

2.10 | In vivo biodistribution of ADSC-EVs

All animal experiments were performed with approval from the Institutional Review Board of Sungkyunkwan University (SKKUIACUC2021-05-02-1). Eight-week-old female ICR (CD-1) mice were purchased from Orientbio, Inc. (Seongnam, Korea). All mice were fed with alfalfa-free feed (Raonbio Co., Ltd, Yongin, Korea) to reduce the autofluorescence before experiments.

At 12-week-old, ICR mice were randomly divided into three groups and intravenously injected with PBS (100 μ l), Cyanine5.5 NHS ester (Lumiprobe, Maryland, USA) (Cy5.5, 5 μ g/ml, 100 μ l), and Cyanine5.5 labelled ASC-EVs (Cy5.5 EVs, 1×10^9 particles/100 μ l PBS). The mice were euthanized at 1, 4, 7, and 25 h after injection, and ex vivo images of bone and major organs were harvested. Time-dependent biodistribution was analysed using IVIS Lumina XR (Caliper Life Sciences, Inc., Hopkinton, MA, USA, the BIORP of Korea Basic Science Institute).

At 9-week-old, ICR mice were bilaterally OVX. Five weeks after OVX, mice were randomly divided into two groups and intravenously injected with Cy5.5 (5 μ g/ml, 100 μ l) and Cy5.5 EVs (1×10^9 particles/100 μ l PBS). Ex vivo images of bone and major organs were harvested at 4 and 7 h after injection using IVIS Lumina XR. OVX mice injected with PBS were used as the negative control for the fluorescence intensity.

All fluorescence images were measured using a Cy5.5 filter set (excitation 640 nm, emission 695–770 nm). An excitation filter at 605 nm was used to measure the autofluorescence. The background filter image was subtracted from the Cy5.5 filter image, and radiant efficiency (p/sec/cm²/sr)/(μ W/cm²) was calculated using Living Image 4.7.3 software (Caliper Life Sciences, Inc., Hopkinton, MA, USA, the BIORP of Korea Basic Science Institute).

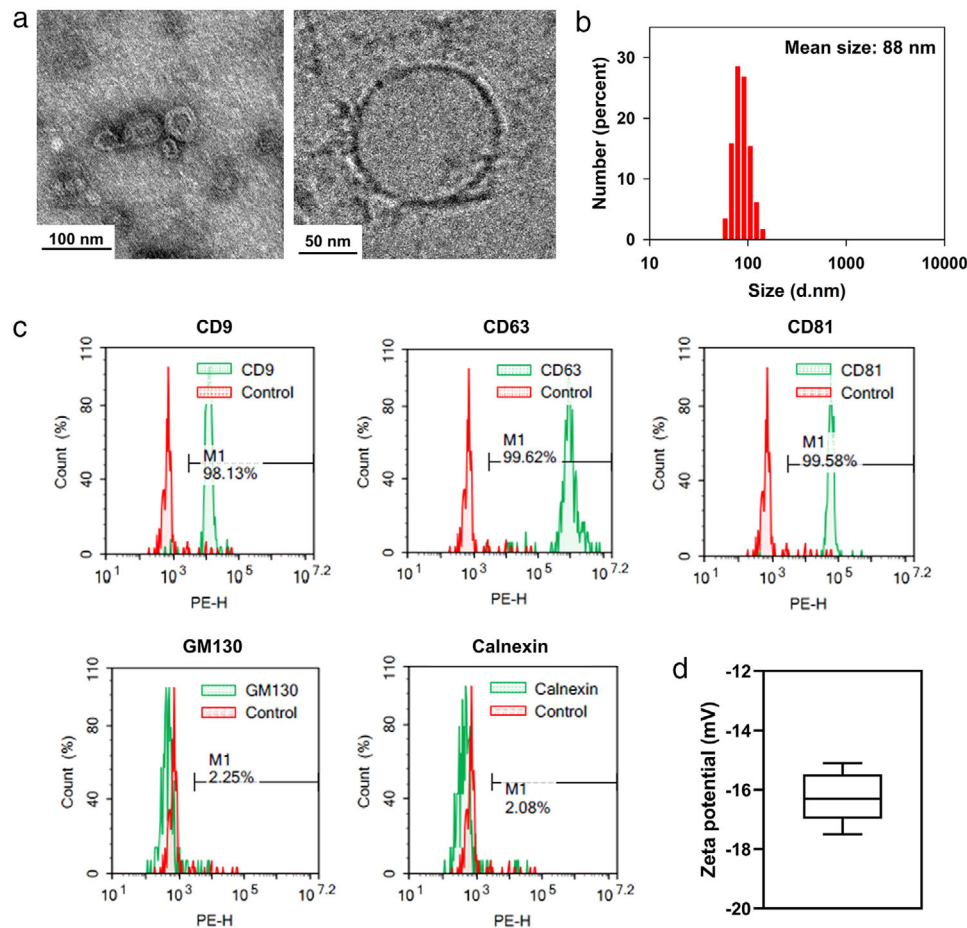


FIGURE 1 Characterization of EVs isolated from human ASCs (ASC-EVs). (a) Classic and cryogenic transmission electron microscopy (TEM) images of ASC-EVs. Scale bar, 100 nm (left) and 50 nm (right). (b) Particle size distribution of ASC-EVs measured by dynamic light scattering. (c) Flow cytometric analysis of EV surface markers (CD9, CD63, and CD81) and internal protein markers (GM130 and calnexin). (d) Zeta potential measurements of ASC-EVs. The mean zeta potential of ASC-EV was -16.3 mV

2.11 | Statistical analysis

Experimental results were expressed as mean \pm standard deviation (SD). The Student's two-tailed *t*-test and one-way analysis of variance with Tukey's post hoc test were performed using GraphPad Prism 8 software (GraphPad, San Diego, CA, USA). $p \leq 0.05$ was considered statistically significant.

3 | RESULTS

3.1 | Characterization of adipose tissue-derived stem cells

ASC-EVs were characterized according to morphology, size distribution, surface markers, and surface charge (Figure 1a–d). ASC-EVs displayed a round shape with a bilayer structure (Figure 1a), and the mean diameter was 88 nm (Figure 1b). Fluorescence-activated cell sorting (FACS) analysis revealed that ASC-EVs were positive for EV markers, including CD9 (98.13%), CD63 (99.62%), and CD81 (99.58%), whereas negative expression of the non-EV markers GM130 (2.25%) and calnexin (2.08%) were observed (Figure 1c). In addition, the mean zeta potential of ASC-EVs was -16.3 ± 0.85 mV (Figure 1d). ASCs were also characterized according to morphology, differentiation potential, and surface markers (Figure S1). The morphology of ASCs was shown (Figure S1A), and their adipogenic and osteogenic differentiation potentials were confirmed using Oil-Red O and Alizarin-Red staining (Figure S1B and S1C). Also, the surface markers were analysed using FACS analysis (Figure S1D–F). CD34 is the ASC marker observed in about 60% of the initial stromal-vascular cell fraction (SVF) cells but gradually decreased as cultured in vitro (Gimble et al., 2007). CD 45, one of the negative markers of ASC, is known as a major histocompatibility complex (MHC) class II marker. On the other hand, CD44, CD73, CD90, and CD105 are all MHC class I markers and are known to be expressed in both

MSCs and ASCs (Kocan et al., 2017). ASCs were negatively stained for CD34 and CD45 and were positively stained for CD44, CD73, CD90, and CD105 (Figure S1E and S1F).

3.2 | Therapeutic efficacy of ASC-EVs in an OVX mouse model

To investigate the therapeutic efficacy of ASC-EVs in OVX mouse models of postmenopausal osteoporosis, OVX mice were intravenously injected with ASCs (5×10^5 cells/100 μ l PBS, once a week for 2 weeks), ASC-EVs (1 or 5×10^8 particles/100 μ l PBS, thrice a week for 2 weeks), or vehicle (PBS). The μ CT images revealed a significant bone loss in the vehicle-injected group compared to those of sham mice. However, the ASC- or ASC-EV-injected group exhibited a remarkable restoration of trabecular bone, and similar results were observed in the 3D reconstruction of mouse femurs (Figures 2a and 2b). For quantifying these changes, the CTvox program was used for bone 3D microarchitecture analysis. As shown in Figure 2, ASC-EV-5 (5×10^8 particles) treatment showed a significant increase in percent change of BMD (71%; $p = 0.0002$), bone volume (105%; $p < 0.0001$), percent bone volume (bone volume over total volume; 98%; $p < 0.0001$), trabecular thickness (97%; $p = 0.0022$), and trabecular number (101%; $p < 0.0001$) compared to the PBS-treated group (Figure 2a–g). The structure model index, which reflects the degree of rods and plates in a 3D structure, was markedly decreased in the ASC-EV-5-treated group (90%; $p = 0.0002$) compared to the PBS-treated group (Figure 2h). Bone marrow density was lower in ASC-EV-injected groups compared to the ASC-treated group, but the values of trabecular thickness were significantly higher ($p = 0.0062$) in the ASC-EV-5-treated group compared to the ASC-treated group (Figures 2c and 2f). The other parameters were not significantly different between the ASC- and ASC-EV-injected groups (Figures 2d, 2e, 2g, and 2h). These results suggested that ASC-EVs inhibit bone loss and promote bone regeneration under osteoporosis conditions.

3.3 | Cytokine composition in ASC-EVs

Cytokines in ASC-EVs were detected using a human bone metabolism array kit (Figures 3a and 3b). Of the total 41 cytokines, eight cytokines involved in osteoblast differentiation, activation, and bone repair were expressed in ASC-EVs, including insulin-like growth factor-1 (IGF-1), interleukin-17 (IL-17), osteoactivin, transforming growth factor- β 1 (TGF- β 1), bone morphogenetic proteins (BMP-6 and BMP-7), OPG, and osteopontin (OPN). Cytokines related to the recruitment and migration of MSCs toward bone resorptive sites were also expressed in ASC-EVs, such as monocyte chemoattractant protein-1 (MCP-1), matrix metalloproteinase (MMP)-2, MMP-3, and tumour necrosis factor- α (TNF- α) (W. Lin et al., 2017; L. Wang et al., 2002). Notably, OPG, which acts as an inhibitor of osteoclast migration and differentiation (Boyce & Xing, 2008; Mizuno et al., 1998), was highly expressed in EVs (46.8 pg/1 $\times 10^8$ EV particles; Figure 3c). Together, ASC-EVs contained various cytokines involved in bone metabolism and MSC migration, and OPG would be a major effector in ASC-EVs.

3.4 | ASC-EVs induce BM-MSc migration

The recruitment and migration of resident BM-MSCs to fracture sites are essential for bone healing (W. Lin et al., 2017; Su et al., 2018). To investigate the effect of ASC-EVs on BM-MSc migration, the transwell migration assay for 18 h was performed (Figure 4a–c). The serum-starved MSCs were loaded on the upper side of the insert. Each lower chamber of the transwell was filled with a medium containing 1×10^8 , 5×10^8 , and 10×10^8 particles/ml EVs. The results showed that ASC-EVs dose-dependently promoted BM-MSc migration to the lower chamber containing ASC-EVs across the membrane (Figures 4b and 4c). These data indicated that ASC-EVs might have bioactive factors related to the recruitment of MSCs, leading to BM-MSc migration.

3.5 | ASC-EVs inhibit osteoclastogenesis

Next, to investigate whether ASC-EVs that contain OPG abundantly can inhibit osteoclast differentiation, RANKL-treated RAW264.7 cells were incubated with ASC-EVs. RANKL induced a high level of osteoclast differentiation, characterized by expressing TRAP specifically and being multinucleated, in RAW264.7 cells in vitro (Figure 5a–c). The combination treatment of OPG with RANKL decreased the formation of TRAP-positive osteoclasts in a dose-dependent manner. ASC-EV treatment also markedly reduced the number of TRAP-positive osteoclasts by 114.0 ± 18.3 , 68.3 ± 11.9 , and 21.3 ± 2.0 at ASC-EV concentrations of 1×10^8 , 5×10^8 , and 10×10^8 particles/ml, respectively. Notably, ASC-EVs treatment of 1×10^9 particles (The amount of OPG in ASC-EVs, 0.5 ng/10⁹ particles) showed a similar inhibitory effect compared to 50 ng/ml OPG. The effect of ASC-EVs on the levels of specific genes for osteoclast and cell proliferation was investigated in RAW264.7 cells (Figure 5d; Figure S2). Quantitative real-time polymerase chain reaction (RT-PCR) showed that the expression levels of tartrate-resistant acid phosphatase 5 (*Acp5*),

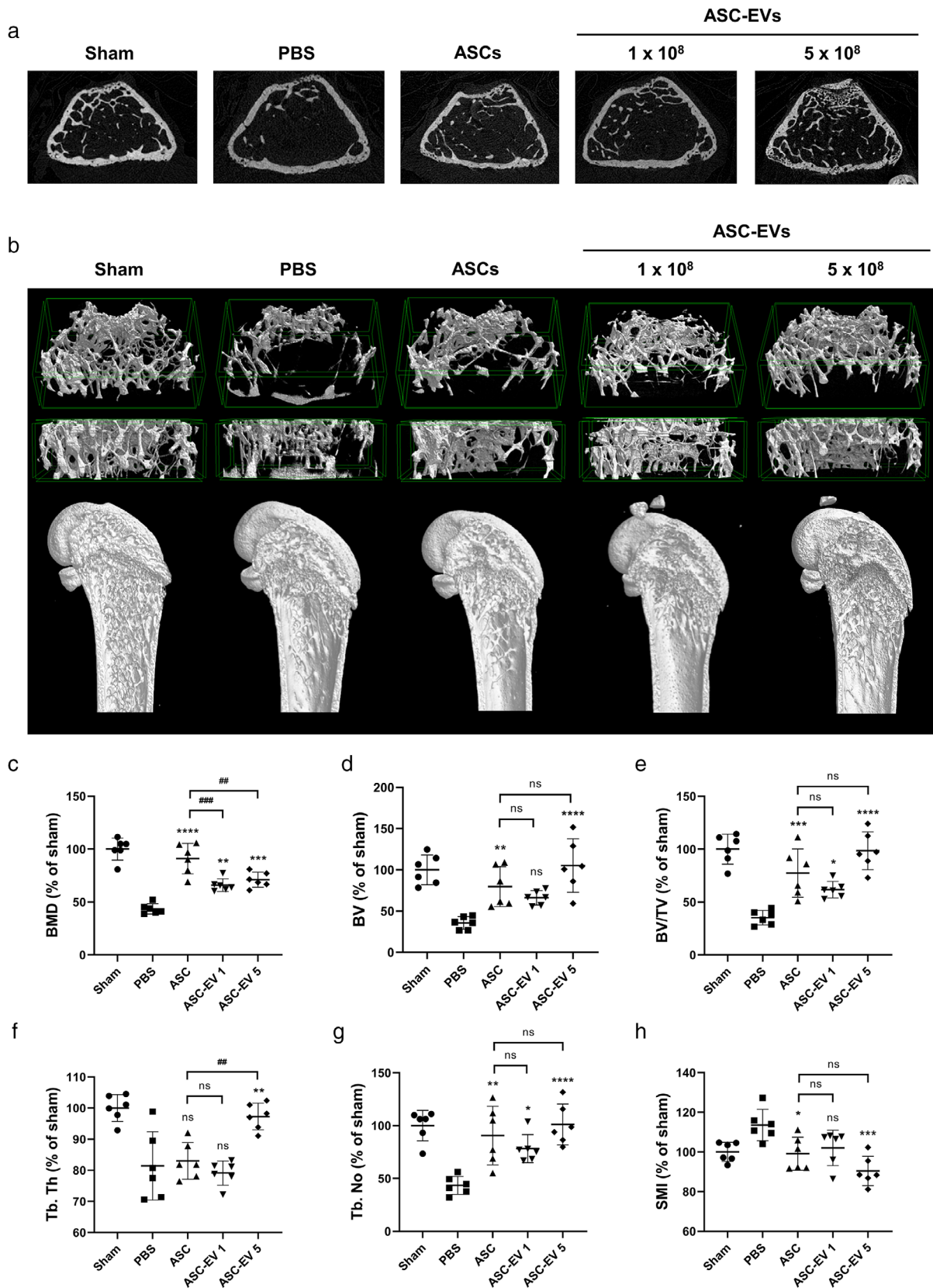


FIGURE 2 Administration of ASC-EVs ameliorates osteoporosis phenotypes in OVX mice. (a) Representative transverse cross-sectional images of trabecular bone and (b) 3D reconstruction images of femora. (c–h) Quantitative analyses of trabecular bone microarchitecture in femora. Four weeks after the first treatment, the left femur was harvested, and trabecular structural indices were measured by μ CT. Data are mean \pm SD ($n = 6$). * $p < 0.05$; ** $p < 0.01$; *** $p < 0.001$; **** $p < 0.0001$; ## $p < 0.01$; ### $p < 0.001$. BV, bone volume; BV/TV, percent bone volume; Tb. Th, trabecular thickness; Tb. No, trabecular number; SMI, structure model index

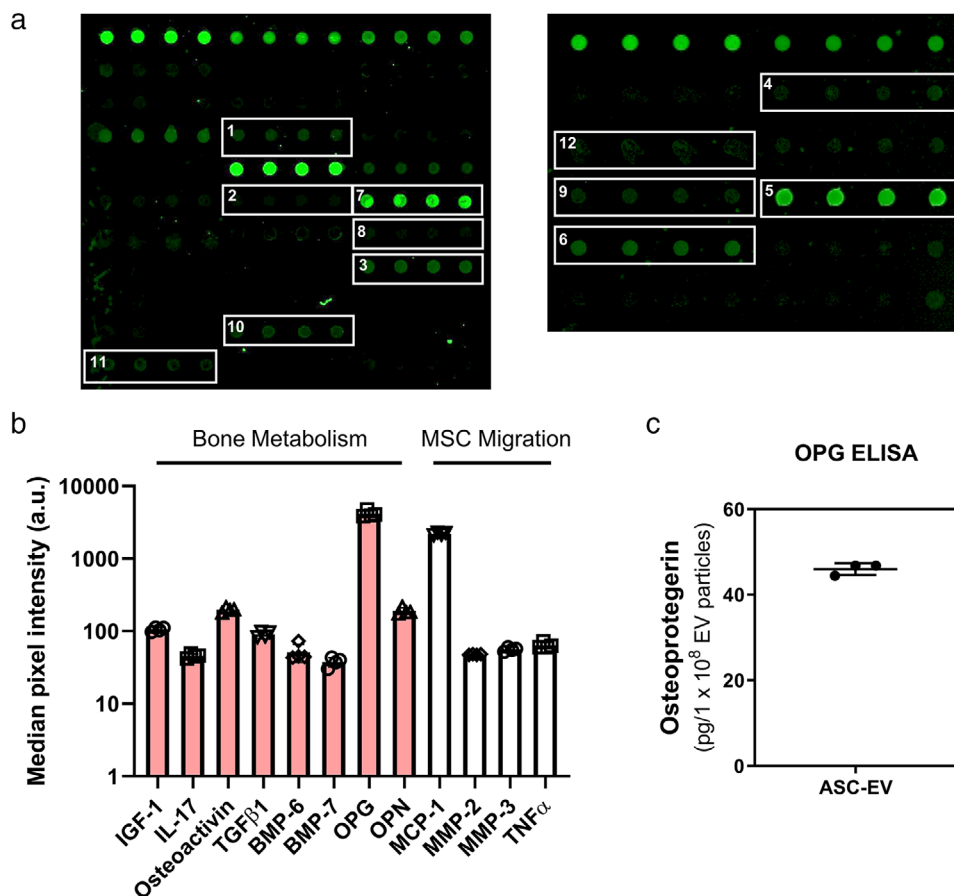


FIGURE 3 Profiling of EV cytokines involved in bone metabolism. (a) Representative fluorescent images of cytokine arrays. (1) IGF-1, (2) IL-17, (3) osteoactivin, (4) BMP-6, (5) OPG, (6) OPN, (7) MCP-1, (8) MMP-2, (9) MMP-3, (10) TGF-β1, (11) TNF-α, and (12) BMP-7. (b) Median pixel intensity of cytokines. (c) Protein expression of OPG determined using enzyme-linked immunosorbent assay (ELISA). Data are mean ± SD

cathepsin K (*Ctsk*), matrix metalloproteinase-9 (*Mmp9*), and nuclear factor of activated T cells 1 (*Nfatc1*) were significantly increased by RANKL but down-regulated in a concentration-dependent manner by OPG. Furthermore, ASC-EV treatment, which contains OPG of 0.5 ng/10⁹ particles, significantly inhibited the expression levels of *Acp5* (0.54-fold), *Ctsk* (0.61-fold), and *Mmp9* (0.35-fold). However, ASC-EVs treatment did not affect the proliferation of RAW264.7 cells (Figure S2). Taken together, ASC-EVs contain key factors that inhibit osteoclastogenesis in RAW264.7 cells.

3.6 | OPG-deprived EVs reduce anti-osteoclastogenesis effects

To further investigate whether the effects of ASC-EVs are dependent on OPG in ASC-EVs, OPG mRNA (TNF Receptor Superfamily Member 11b [*TNFRSF11B*], encoding OPG) and protein were knocked down using lentiviral small hairpin RNA (lenti-shRNA) in ASCs (Figure 6a–c; Figure S3A) (Stewart, 2003). Then, conditioned media (CM) from control ASCs and OPG knock-down ASCs were collected, and EVs were isolated from CM (Figure S3D and S3E). The amount of OPG was markedly reduced in OPG knockdown ASC-EVs (OPG KD-EVs) compared to control ASC-EVs (Con-EVs; Figures 6c and 6d; Figure S3B and S3C). To compare the effects of Con-EVs and OPG KD-EVs in anti-osteoclastogenesis, osteoclast differentiation in RAW264.7 cells treated with Con-EVs or OPG KD-EVs was induced by treatment with RANKL (Figures 6e and 6f). TRAP-positive and multinucleated cells were reduced in RAW264.7 cells treated with Con-EVs. In contrast, OPG KD-EVs failed to lessen osteoclastogenesis in RAW264.7 cells treated with RANKL. Also, the expression level of mRNAs related to the RANKL-RANK signalling pathway was significantly reduced in RAW264.7 cells treated with Con-EVs (Figure 6g). Unexpectedly, OPG KD-EVs also partially reduced the RANKL-RANK signalling pathway, except for *Nfatc1*, compared to the group only treated with RANKL. However, the inhibitory effects were greater in Con-EV-treated groups than OPG KD-EV-treated groups. Next, the effects of OPG KD-EVs in osteoporosis were tested in vivo model. OVX mice were intravenously injected with OPG KD-EVs three times a week for 2 weeks. The micro-CT analysis showed a significant bone loss in the PBS-injected OVX group compared to the sham group (Figure S4A). Restoration of trabecular bones was found in the ASC-EVs-injected group, but there was no difference in OPG

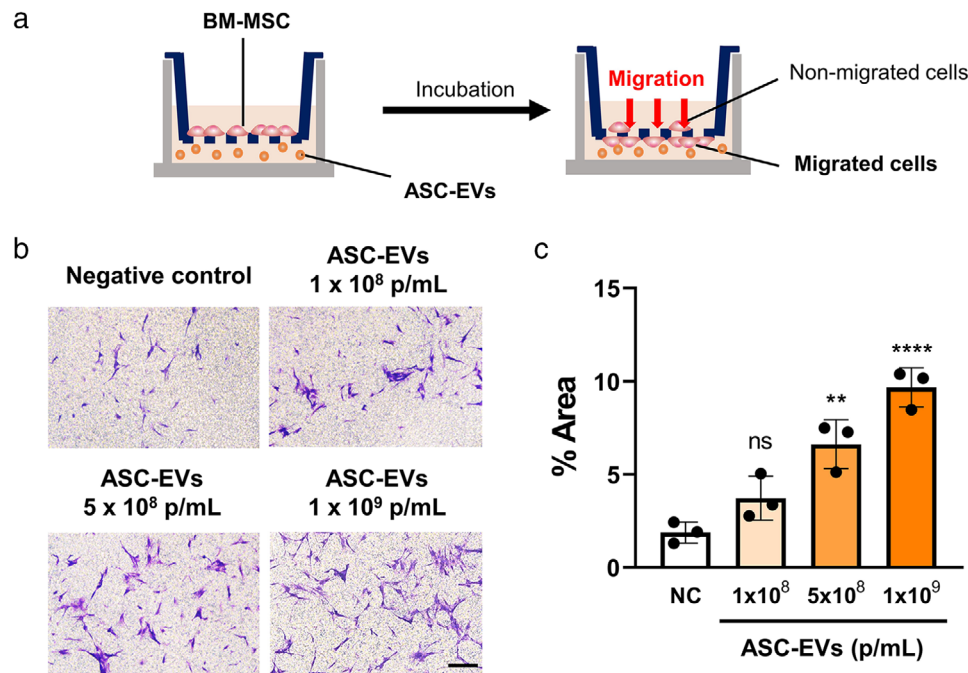


FIGURE 4 Effect of ASC-EVs on BM-MSC migration. (a) Schematic representations of transwell migration assay. BM-MSCs were seeded into the upper side of the transwell membrane. The medium containing various concentrations of ASC-EVs was placed in the lower side chamber of the transwell plate. (b) After 18 h, migrated cells to the lower side were fixed with 4% paraformaldehyde and stained with crystal violet. Scale bar, 200 μ m. (c) Percent area of migrated cells quantified using ImageJ software. Data are mean \pm SD (n = 3). ** p < 0.01; **** p < 0.0001

KD-EV-injected group compared to the PBS-injected group (Figure S4B–G). Thus, ASC-EVs inhibit osteoclast differentiation induced by RANKL and attenuate the bone loss in OVX mice dependent on OPG in ASC-EVs.

3.7 | miRNAs associated with osteoporosis were present in ASC-EVs

Because OPG-depleted ASC-EVs showed a reduced anti-osteoclastogenesis effect and ASC-EVs produced the same results with a smaller amount of OPG, it was hypothesized that other factors of ASC-EVs also contribute to the inhibition of osteoclast differentiation. It has been reported that miRNAs were involved in regulating bone remodelling processes and function (Lian et al., 2012). Also, numerous miRNAs have been reported to be changed in osteoporotic patients compared to non-osteoporotic patients (Bottani et al., 2019; Ciuffi et al., 2020; Materozzi et al., 2018). Thus, miRNA expression profiles in ASC-EVs were assessed to find the candidates associated with the anti-osteoclastogenesis effects of ASC-EVs. The most abundant miRNAs in ASC-EVs were listed according to the reads per million mapped reads (RPM; Figure 7a). Whether down-regulated miRNAs in osteoporotic patients were decreased in RAW264.7 cells by treatment with RANKL was confirmed (Figure 7b; Figure S5A). The *miR-21-5p* expression level was reduced by treatment with RANKL, and the reduction was attenuated by co-treatment with ASC-EVs. Furthermore, the presence of miRNAs in ASC-EVs was validated using droplet digital PCR (ddPCR; Figure 7c; Figure S5B). ddPCR calculates the concentration by classifying positive and negative droplets according to the target DNA amplification and analysing the ratio of positive to negative droplets according to Poisson's distribution (Stein et al., 2017). With this system, 40.6 copies/ μ L PCR was measured for *hsa-miR-21-5p* in ASC-EVs. Also, the expression level of *Pten*, which is a known target of *miR-21-5p*, was decreased by the treatment of ASC-EVs (Figure S6A) (Meng et al., 2007). Then, targets of *miR-21-5p* were predicted using TargetScan 7.2 and miRDB (Table S2). Some of them were related to osteoclast differentiation, such as activin receptor type 2A (ACVR2A), activin receptor type 1c (ACVR1C, also known as ALK7), B-cell translocation gene 2 (BTG2, also known as TIS21), and interferon-related developmental regulator 1 (IFRD1). Activin-A binds to activin receptor type II (ACVR2) and activin receptor type I (ACVR1) sequentially and activated ACVR1 phosphorylates SMAD2/3, leading to the expression of target genes and osteoclast differentiation (Kajita et al., 2018; Morianos et al., 2019; Schoenmaker et al., 2020). Also, the expression levels of BTG2 and IFRD1 were increased in mature osteoclasts, and inhibiting BTG2 and IFRD1 reduced the osteoclast differentiation (Iezaki et al., 2016; Lee et al., 2002). The target genes of *miR-21-5p* were increased in treatment with RANKL and attenuated with the treatment of ASC-EVs (Figure 7d; Figure S5C). Next, to confirm that *miR-21-5p* regulates the expression of *Acvr2a* and osteoclast differentiation, pre-miR-21 was transfected in RAW264.7 cells with the treatment of RANKL. The expression levels of *Acvr2a*

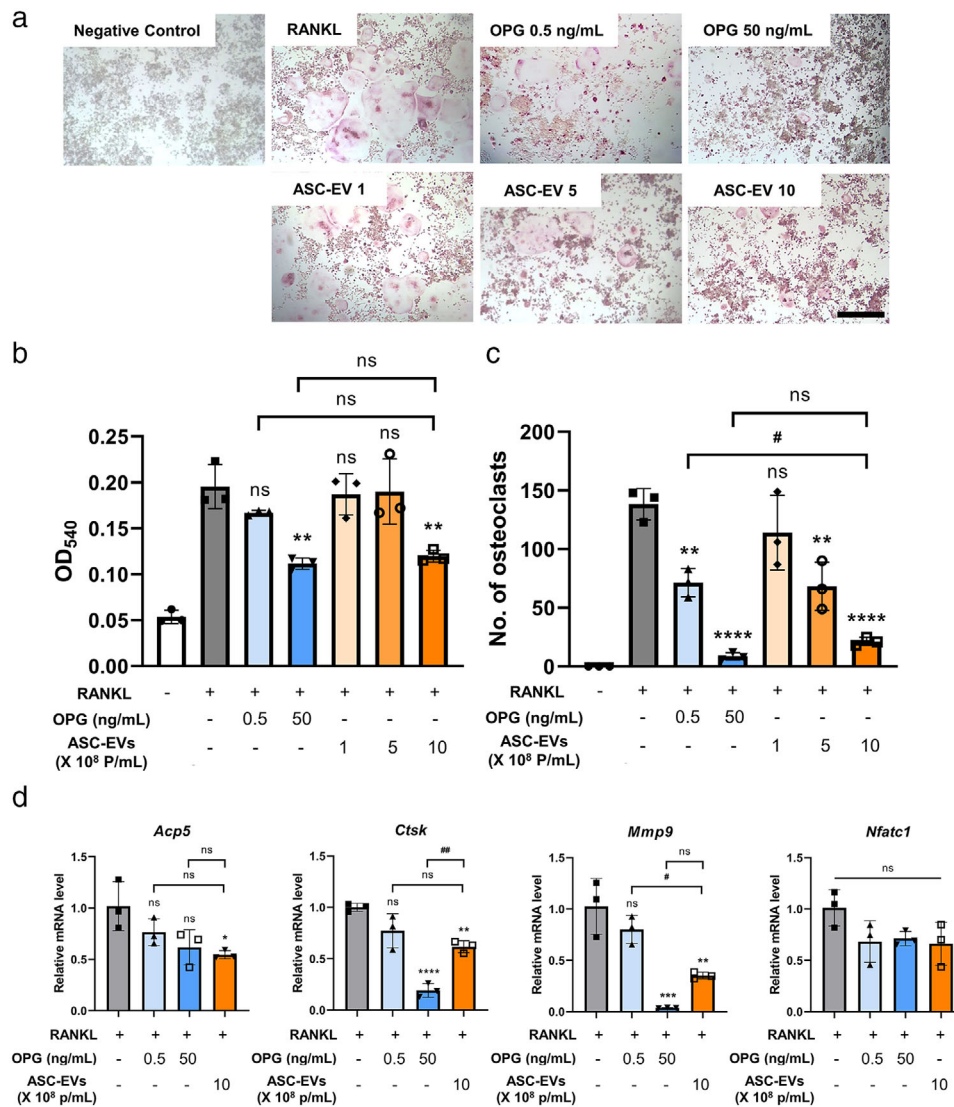


FIGURE 5 Inhibitory effect of ASC-EVs on osteoclast differentiation of RAW264.7 cells. (a) TRAP staining of RAW264.7 cells after 6 days of incubation with RANKL containing medium supplemented with OPG (0.5 or 50 ng/ml) or ASC-EVs (1×10^8 – 10×10^8 particles/ml) for 6 days. Scale bar, 200 μ m. (b) TRAP activity in culture supernatants was assessed by measuring the optical density at 540 nm. (c) The number of TRAP-positive multinucleated cells was observed under a light microscope and counted. (d) The gene expression associated with osteoclastogenesis in RAW264.7 cells was determined by qPCR. The relative gene expression was normalized to a housekeeping gene [glyceraldehyde 3-phosphate dehydrogenase (*Gapdh*)] and expressed as the fold change compared to RANKL-treated RAW264.7 cells. Data are mean \pm SD (n = 3). * p < 0.05; ** p < 0.01; *** p < 0.001; **** p < 0.0001; # p < 0.05; ## p < 0.01

were decreased, and the number of osteoclasts was significantly reduced by overexpressed *miR-21-5p* (Figure 7e; Figure S6B–D). Also, the expression levels of *Acp5* and *Ctsk*, related to the osteoclast differentiation, were significantly reduced in RAW264.7 cells transfected with pre-miR-21, but not *Mmp9* and *Nfact1* (Figure 7g). On the other hand, the expression levels of *Acvr2a* and *Nfatc1* were significantly increased by the transfection of anti-miR-21, but there was no difference in the expression levels of *Ctsk* and *Mmp9* compared to the group treated with RANKL and ASC-EVs (Figures S6E and S6F). Furthermore, the effects of *let-7b-5p* were also investigated since its expression level was decreased in RANKL treatment and was restored by the treatment of ASC-EVs (Figure S5A). The expression levels of genes related to the RANK-RANKL signalling pathway were significantly decreased by the overexpressed *let-7b-5p* compared to the group only treated with RANKL (Figure S6G). The predicted pairings of target regions and miRNA were described (Figure 7f; Figure S5D). To examine how miRNAs in ASC-EVs were delivered to cells, the cellular uptake of EVs was investigated. RAW264.7 cells were incubated with 1×10^9 particles/ml PKH67-labelled ASC-EVs for 12 h. ASC-EVs were internalized into the cytoplasm of RAW264.7 cells (Figure 7h). These results implied that ASC-EVs are successfully transferred into RAW264.7 with high cellular uptake efficiency. Together, these data supported that another therapeutic pathway of ASC-EVs involves inhibiting osteoclast differentiation by transferring *miR-21-5p* through *Acvr2a* down-regulation.

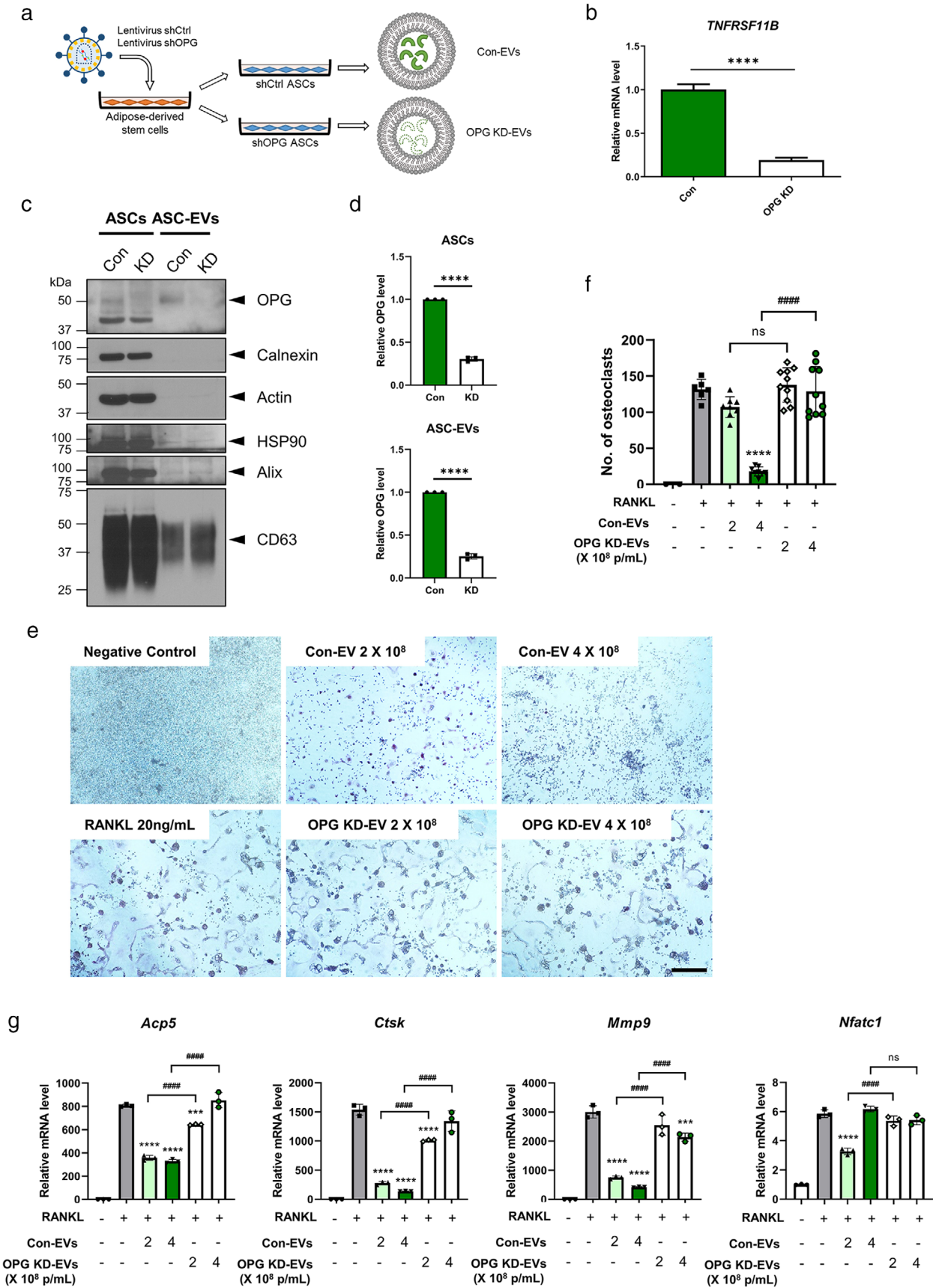


FIGURE 6 OPG-dependent anti-osteoclastogenesis effects of ASC-EVs. (a) Strategies to identify that anti-osteoclastogenesis effects of ASC-EVs are dependent on OPG. (b) OPG mRNA (*TNFRSF11B*) level in lentiviral control shRNA-transduced ASCs (shCtrl ASCs) and lentiviral OPG shRNA-transduced

3.8 | Adipose tissue-derived stem cells are delivered to bone tissue

To investigate the *in vivo* biodistribution of ASC-EVs, the Cyanine5.5-labelled ASC-EVs (Cy5.5 EVs) were injected intravenously into the ICR mice (Figures S7A and S7B). *Ex vivo* images of bone and major organs were harvested at 1, 4, 7, and 25 h after injection. The fluorescence intensity of the Cy5.5 EVs-injected group was higher than that of the free Cyanine5.5 dye (Cy5.5)—injected group in bone tissue, and the intensity was strong at 4 and 7 h after injection (Figure S7A). At 1 h after injection, the Cy5.5-injected group showed a stronger intensity in the liver tissue than the Cy5.5 EVs-injected group, but the fluorescence intensity was decreased faster in the Cy5.5-injected group over time (Figure S7B). Then, the Cy5.5 EVs were injected intravenously into the OVX mice, and *ex vivo* images of bone and major organs were harvested at 4 and 7 h after injection (Figure 8; Figure S7C–E). Cy5.5 EVs-injected group showed significantly higher fluorescence intensity than Cy5.5-injected group in bone tissue at both 4 and 7 h after injection (Figures 8a and 8b). Also, the fluorescence intensity of all major organs was significantly stronger in the Cy5.5 EVs- than in the Cy5.5-injected group (Figure 8c–e). The fluorescence intensity was not detected in the bone tissue, and major organs of PBS injected mouse, and all attached muscle tissue was removed (Figure S7C–E). These results showed that ASC-EVs reach the bone tissue after being injected intravenously, and they remain longer in major organs.

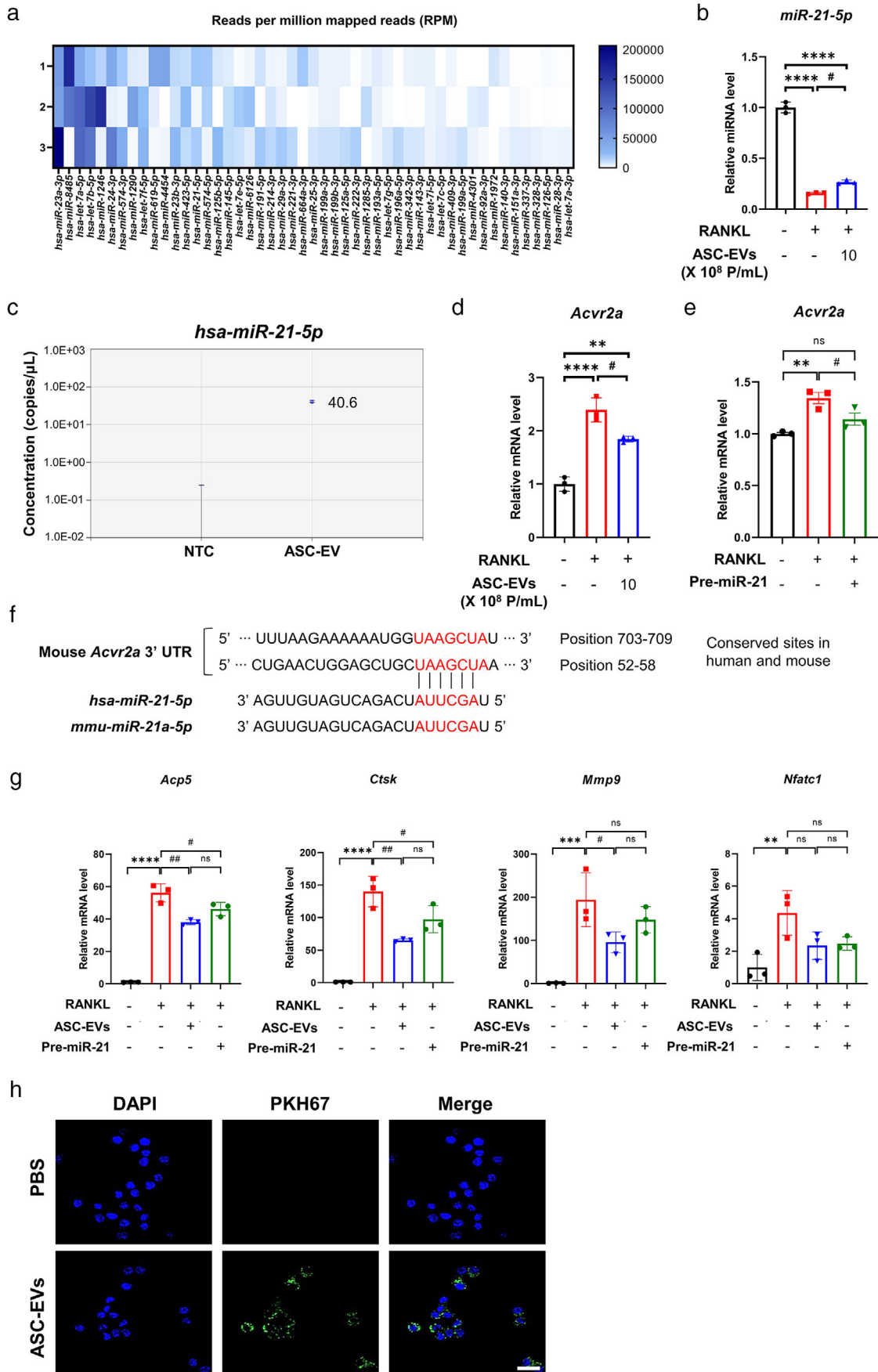
4 | DISCUSSION

Many studies have supported the roles of EVs in intercellular communication through paracrine signalling in osteoporosis. As essential components of EVs, miRNAs and proteins have attracted much attention in EV function studies. Qin et al. reported that BM-MSC-derived EVs regulate osteoblast activity and differentiation by *miR-196a* *in vitro* and *in vivo* (Qin et al., 2016). Li et al. found that osteoclast-derived EV *miR-214-3p* inhibits osteogenic activity and bone formation (D. Li et al., 2016). In another study, osteoblast-derived EVs contain bone regulatory proteins that stimulate osteoclast formation, such as RANKL and parathyroid hormone (Deng et al., 2015). Moreover, Chen et al. reported that collagen triple-helix repeat-containing 1 and OPG enriched in EVs derived from human urine-derived stem cells regulate osteogenesis and osteoclastogenesis (C.-Y. Chen, Rao, et al. 2019).

In this study, ASC-EVs could effectively alleviate bone loss in OVX-induced osteoporotic mice (Figures 2). The systemic administration of ASC-EVs showed a significant recovery of structural parameters, including BMD, bone volume, trabecular thickness, which was comparable to ASC administration's therapeutic effects. These results indicated that ASC-EVs have similar protective and regenerative functions as ASC transplantation in OVX-induced bone loss. Compared to stem cell transplantation, EV therapy is desirable for clinical applications because of its advantages, such as low immunogenicity, improved safety, ease of storage and management, and mass production (Lener et al., 2015; Yeo et al., 2013).

Here, two concepts of inhibiting bone resorption and recruiting BM-MSCs into defect sites demonstrate the therapeutic effect of ASC-EVs (Figure S8). First, the growth factors and cytokines related to bone metabolism and MSC migration in the EVs were analysed (Figure 3). ASC-EVs contained various cytokines that stimulate MSC migration to the bone resorptive sites (MCP-1, MMP-2, MMP-3, TGF- β 1, TNF- α , and BMP-7) (Kempen et al., 2010; W. Lin et al., 2017; L. Wang et al., 2002) and promote osteoblast differentiation, activation, and bone formation (IGF-1, IL-17, osteoactivin, BMP-6, BMP-7, OPG, and OPN) (D. Li et al., 2016; Kempen et al., 2010; Su et al., 2018). Among the detected growth factors and cytokines, OPG was most highly expressed in ASC-EVs. OPG is primarily expressed by bone marrow stromal cells and osteoblasts (M. R. Mcclung, 2006). OPG binds to RANKL with an approximately 500-fold higher affinity than RANK, inhibiting osteoclastogenesis and excessive osteoclast-mediated resorption (Nelson et al., 2012). Indeed, *in vitro* studies showed that ASC-EVs effectively stimulate BM-MSC migration and suppress osteoclastogenesis of RAW264.7 cells without adverse effects (Figures 4 and 5). These results supported the assertion that EV cytokines effectively contribute to OVX-induced bone loss recovery by stimulating BM-MSC migration and inhibiting osteoclast differentiation. Next, to demonstrate that OPG in ASC-EVs is a significant player that blocks osteoclast differentiation, OPG expression was knocked down using lentiviral shOPG in ASC (Figure 6). Then, EVs were isolated from OPG-depleted ASC CM, and the effects of ASC-EVs and OPG-depleted ASC-EVs were compared. ASC-EVs inhibited osteoclastogenesis significantly, but OPG-depleted ASC-EVs did not reduce osteoclast differentiation and bone loss. Furthermore, miRNAs included in ASC-EVs were analysed because OPG-depleted ASC-EVs still partially reduced gene expression related to the RANKL-RANK pathway, and ASC-EVs showed the same effects with a smaller amount of OPG. *miR-21-5p* existed in ASC-EVs and was reduced in RANKL-induced RAW264.7 cells. *Acvr2a*, a predicted target of *miR-21-5p*, was increased by treatment with RANKL and decreased by treatment with ASC-EVs (Figure 7). These results link two previous reports. First, levels of *miR-21-5p* were reduced

ASCs (shOPG ASCs). The relative OPG mRNA level was normalized to a housekeeping gene (*18S*) and expressed as the fold change compared to shCtrl ASCs. (c) Western blot representative images of shCtrl ASCs, shOPG ASCs, ASC-EVs (Con-EVs), and OPG-depleted ASC-EVs (OPG KD-EVs). (d) The relative OPG protein expression was quantified in ASCs and ASC-EVs using ImageJ software. The relative protein expression was normalized to Actin in ASCs and CD63 in ASC-EVs. (e and f) TRAP staining representative images (e) and quantification of osteoclastogenesis in RAW264.7 cells (f). Scale bar, 500 μ m. (g) The gene expression in RAW264.7 cells was determined by qPCR. The relative gene expression was normalized to a housekeeping gene (*Gapdh*) and expressed as the fold change compared to RANKL-untreated RAW264.7 cells. Data are mean \pm SD. *** p < 0.001; **** p < 0.0001; #### p < 0.0001



in osteoporosis patients (Bottani et al., 2019; Ciuffi et al., 2020; Materozzi et al., 2018). Second, deletion of *ACVR2A* in osteoblast increased its differentiation, and *ACVR2A* knockout mice showed the increased bone volume (Goh et al., 2017). Indeed, *miR-21* promoted osteogenic differentiation by inhibiting translation of *SMAD7* (H. Li et al., 2015), and *miR-21-5p* was recently suggested as a therapeutic target for osteoporosis (Huang et al., 2021). *let-7b-5p*, as well as *miR-21-5p*, was also decreased in the treatment of RANKL and attenuated in the treatment of ASC-EVs. Moreover, it regulated the expression of genes related to osteoclast differentiation (Figures S5 and S6). Finally, ASC-EVs were delivered to the bone tissue when injected into the mice intravenously (Figure 8).

FIGURE 7 miRNA associated with osteoporosis present in ASC-EVs. (a) Heatmap representing the mean RPM across replicates ($n = 3$). miRNAs in ASC-EVs were quantified, and miRNA annotated reads were normalized to RPM. (b) The expression levels of *miR-21-5p* in RAW264.7 cells were determined by qPCR. The relative gene expression was normalized to *miR-16-5p* and *Gapdh* and expressed as the fold change compared to RANKL-untreated RAW264.7 cells. (c) The *miR-21-5p* level in ASC-EVs was measured by ddPCR and presented as copies/ μ L PCR. (d) The predicted target gene of *miR-21-5p* was determined by qPCR in RAW264.7 cells. The relative gene expression was normalized to a housekeeping gene (*Gapdh*) and expressed as the fold change compared to RANKL-untreated RAW264.7 cells. (e) The expression levels of *Acvr2a* in RAW264.7 cells were determined by qPCR. The relative gene expression was normalized to a housekeeping gene (*Gapdh*) and expressed as the fold change compared to RANKL-untreated RAW264.7 cells. (f) Predicted target sites of *Acvr2a* 3'UTR. Red letters showed the predicted pairing of the target region and miRNA. (g) The gene expression in RAW264.7 cells was determined by qPCR. The relative gene expression was normalized to a housekeeping gene (*Gapdh*) and expressed as the fold change compared to RANKL-untreated RAW264.7 cells. (h) Cellular uptake of ASC-EVs into RAW264.7 cells. Images of PKH-67-labeled ASC-EVs (green) with DAPI (blue) were visualized by merging the confocal images. Scale bar, 20 μ m. Data are mean \pm SD. $*p < 0.01$; $***p < 0.001$; $****p < 0.0001$; $\#p < 0.05$; $\#\#p < 0.01$

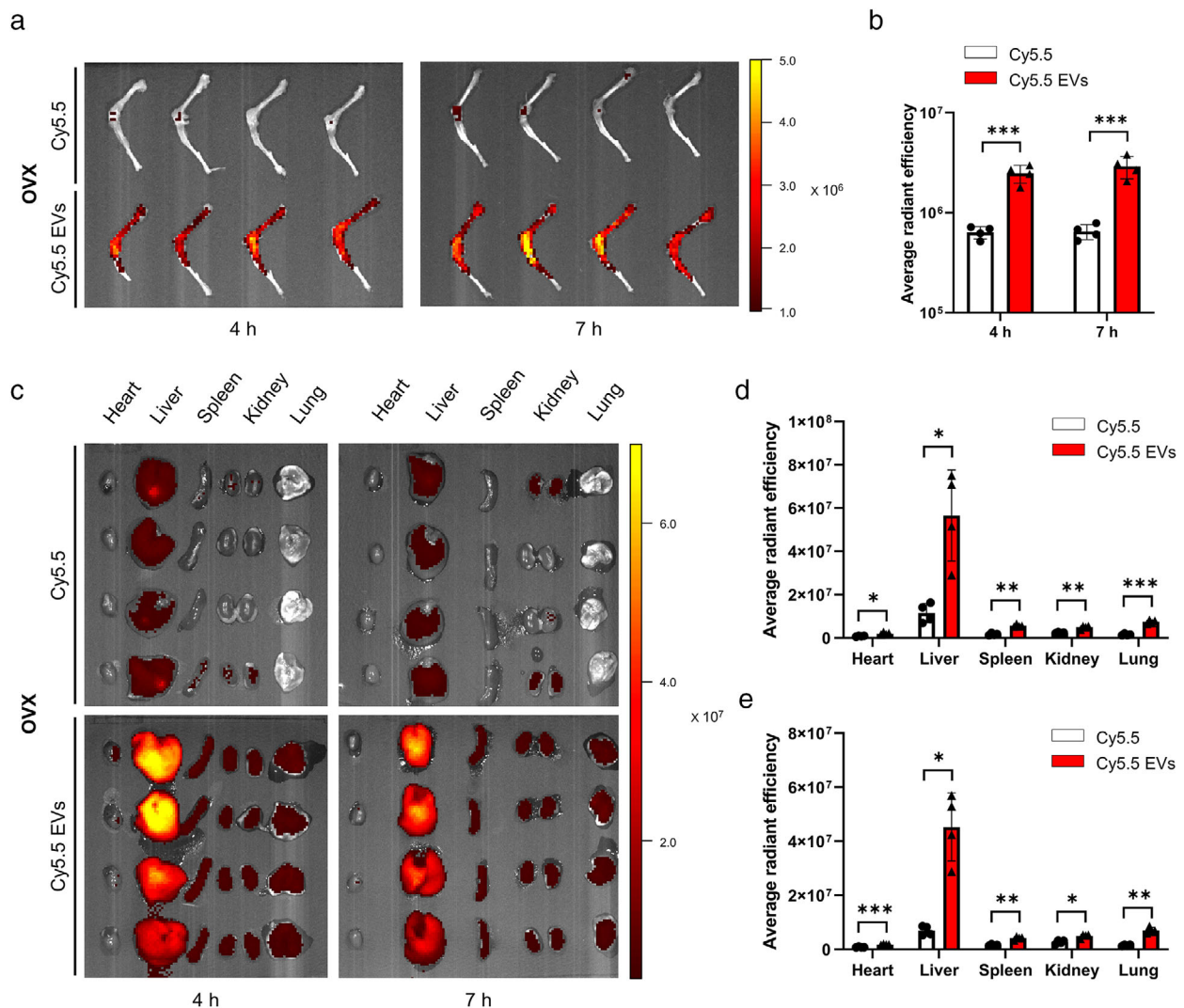


FIGURE 8 In vivo distribution of ADSC-EVs in OVX mice. (a and b) Ex vivo bone distribution images (a) and quantification of fluorescence intensity (b) in OVX mice injected with Cy5.5 EVs or Cy5.5. Ex vivo images of bone tissues were harvested at 4 and 7 h after injection. (c–e) Ex vivo distribution images of major organs (heart, liver, spleen, kidney, and lung) (c) and quantification of fluorescence intensity at 4 h (d) and 7 h (e) after injection with Cy5.5 EVs or Cy5.5. Data are mean \pm SD ($n = 4$). $*p < 0.05$; $**p < 0.01$; $***p < 0.001$

Although this study focused on OPG and *miR-21-5p* in ASC-EVs, it is possible that other components also have partially beneficial effects in osteoporosis. BM-MSC-derived EVs induced osteogenic differentiation and improved bone repair (Narayanan et al., 2016; Qin et al., 2016), and the miRNA expression profile in EVs was changed during osteoblast differentiation (Xu et al., 2014; Zhao et al., 2016). We found that ASC-EVs stimulate the BM-MSC migration, but the effects of ASC-EVs on osteogenic differentiation remain to be investigated. *let-7a*, *miR-199b*, and *miR-196a* are abundant in ASC-EVs, and these miRNAs could be involved in the regulation of osteoblast differentiation (Choi et al., 2019; Qin et al., 2016; Zhao et al., 2016). Also, further mechanistic details of how ASC-EVs are transferred to the cells and bone tissues remain to be elucidated. CD44, a hyaluronan receptor, is expressed on the surface of ASC-EVs. Ragni et al. reported that CD44 is involved in the recruitment and uptake of ASC-EVs, and increasing CD44 on ASC-EVs induced their internalization (Ragni et al., 2019). By culturing ASCs on hyaluronan-coated surfaces, ASC-EVs with increased CD44 levels are harvested, and they could increase the therapeutic efficacy in osteoporosis.

In summary, ASC-EVs can effectively reduce bone loss in OVX mice. ASC-EVs promoted BM-MSC migration and suppressed osteoclast differentiation of RAW264.7 cells through the transfer of diverse cytokines and miRNAs in EVs. Therefore, bone metabolism-related cytokines and miRNAs enriched in ASC-EVs could synergistically contribute to bone remodelling, and ASC-EVs are up-and-coming therapeutic agents for osteoporosis treatment.

ACKNOWLEDGEMENTS

This work was supported by the National Research Foundation (NRF) under Grant NRF-2018M3A9H1023767, NRF-2019RIA5A2027340; NRF-2019RIA2C3011422); Ministry of Food and Drug Safety under Grant (18172MFDS173); and the startup commercialization funded by the Ministry of SMEs and Startups (MSS, Korea). This work was also supported by a grant from the Ministry of Oceans and Fisheries' R&D project, Korea (1525011845), and Korea Basic Science Institute (National Research Facilities and Equipment Center) grant funded by the Ministry of Education (2020R1A6C101A191).

CONFLICTS OF INTEREST

J.H.P., Y.W.C., and D.G.J. are stockholders of Exostemtech, Inc. J.S.C., K.S.L., S.H.Y., C.H.W., Y.J.J., and S.Y.P. are employed by Exostemtech, Inc. The other authors have no conflicts of interest to declare.

AUTHOR CONTRIBUTIONS

Kyoung Soo Lee and Jeongmi Lee designed and performed most of the experiments, analysed the data, and wrote the manuscript. Seung Ho Yeom performed the in vivo experiments. Chang Hee Woo, Youn Jae Jung, Ye Eun Yun, and So Young Park performed the experiments and analysed the data. Hark Kyun Kim, Jihoon Han, Eunae Kim, Jae Hoon Sul, and Jae Min Jung contributed to EV isolation and characterization. Ji Suk Choi and Jae Hyung Park contributed to the design of the study and discussed the results. Yong Woo Cho and Dong-Gyu Jo designed the study, analysed the data, financed the project, directed the project, and wrote the manuscript.

ETHICS APPROVAL

All animal experiments were approved by the Institutional Animal Care and Use Committee (IACUC) of Hanyang University (approval no. HYIACUC 2017-0050A) and Sungkyunkwan University (approval no. SKKUIACUC2021-04-38-1 and SKKUIACUC2021-05-02-1).

DATA AVAILABILITY STATEMENT

The data that support the findings of this study are available from the corresponding author upon reasonable request.

ORCID

Kyoung Soo Lee  <https://orcid.org/0000-0002-3494-0290>

Jeongmi Lee  <https://orcid.org/0000-0002-4134-5713>

Hark Kyun Kim  <https://orcid.org/0000-0003-2755-0806>

Seung Ho Yeom  <https://orcid.org/0000-0003-4101-2190>

Chang Hee Woo  <https://orcid.org/0000-0003-2365-3269>

Youn Jae Jung  <https://orcid.org/0000-0002-4238-9371>

Ye Eun Yun  <https://orcid.org/0000-0001-9676-1020>

So Young Park  <https://orcid.org/0000-0002-3461-8525>

Jihoon Han  <https://orcid.org/0000-0001-5870-1414>

Eunae Kim  <https://orcid.org/0000-0002-8930-8882>

Jae Hoon Sul  <https://orcid.org/0000-0002-0862-7057>

Jae Min Jung  <https://orcid.org/0000-0003-0819-7226>

Jae Hyung Park  <https://orcid.org/0000-0002-5043-9455>

Ji Suk Choi  <https://orcid.org/0000-0002-2351-0316>

Yong Woo Cho  <https://orcid.org/0000-0002-2075-4147>

Dong-Gyu Jo  <https://orcid.org/0000-0003-2271-1076>

REFERENCES

- Antebi, B., Pelled, G., & Gazit, D. (2014). Stem cell therapy for osteoporosis. *Current Osteoporosis Reports*, 12(1), 41–47. <https://doi.org/10.1007/s11914-013-0184-x>
- Biancone, L., Bruno, S., Deregibus, M. C., Tetta, C., & Camussi, G. (2012). Therapeutic potential of mesenchymal stem cell-derived microvesicles. *Nephrology, Dialysis, Transplantation*, 27(8), 3037–3042. <https://doi.org/10.1093/ndt/gfs168>
- Bottani, M., Banfi, G., & Lombardi, G. (2019). Perspectives on MiRNAs as epigenetic markers in osteoporosis and bone fracture risk: A step forward in personalized diagnosis. *Frontiers in Genetics*, 10, 1044. <https://doi.org/10.3389/fgene.2019.01044>
- Boyce, B. F., & Xing, L. (2008). Functions of RANKL/RANK/OPG in bone modeling and remodeling. *Archives of Biochemistry and Biophysics*, 473(2), 139–146. <https://doi.org/10.1016/j.abb.2008.03.018>
- Bruno, S., Deregibus, M. C., & Camussi, G. (2015). The secretome of mesenchymal stromal cells: Role of extracellular vesicles in immunomodulation. *Immunology Letters*, 168(2), 154–158. <https://doi.org/10.1016/j.imlet.2015.06.007>
- Caplan, A. I., & Dennis, J. E. (2006). Mesenchymal stem cells as trophic mediators. *Journal of Cellular Biochemistry*, 98(5), 1076–1084. <https://doi.org/10.1002/jcb.20886>
- Chen, C.-Y., Rao, S.-S., Tan, Yi-J., Luo, M.-J., Hu, X-Ke, Yin, H., Huang, J., Hu, Y., Luo, Z.-W., Liu, Z.-Z., Wang, Z.-X., Cao, J., Liu, Yi-W., Li, H.-M., Chen, Y., Du, W., Liu, J.-H., Zhang, Y., Chen, T.-H., ... Xie, H. (2019). Extracellular vesicles from human urine-derived stem cells prevent osteoporosis by transferring CTHRC1 and OPG. *Bone Research*, 7(1), 18. <https://doi.org/10.1038/s41413-019-0056-9>
- Chen, S., Tang, Y., Liu, Y., Zhang, P., Lv, L., Zhang, X., Jia, L., & Zhou, Y. (2019). Exosomes derived from MiR-375-overexpressing human adipose mesenchymal stem cells promote bone regeneration. *Cell Proliferation*, 52(5), 1–14. <https://doi.org/10.1111/cpr.12669>
- Cho, S. W., Sun, H. J., Yang, J.-Y., Jung, J. Y., Choi, H. J., An, J. H., Kim, S. W., Kim, S. Y., Park, K.-J., & Shin, C. S. (2012). Human adipose tissue-derived stromal cell therapy prevents bone loss in ovariectomized nude mouse. *Tissue Engineering Part A*, 18(9–10), 1067–1078. <https://doi.org/10.1089/ten.tea.2011.0355>
- Choi, S.-Y., Han, E.-C., Hong, Su-H., Kwon, T.-G., Lee, Y., & Lee, H.-J. (2019). Regulating osteogenic differentiation by suppression of exosomal MicroRNAs. *Tissue Engineering Part A*, 25(15–16), 1146–1154. <https://doi.org/10.1089/ten.tea.2018.0257>
- Ciuffi, S., Donati, S., Marini, F., Palmigni, G., Luzi, E., & Brandi, M. L. (2020). Circulating MicroRNAs as novel biomarkers for osteoporosis and fragility fracture risk: Is there a use in assessment risk? *International Journal of Molecular Sciences*, 21(18), 6927. <https://doi.org/10.3390/ijms21186927>
- Deng, L., Wang, Y., Peng, Y., Wu, Yu, Ding, Y., Jiang, Y., Shen, Z., & Fu, Q. (2015). Osteoblast-derived microvesicles: A novel mechanism for communication between osteoblasts and osteoclasts. *Bone*, 79, 37–42. <https://doi.org/10.1016/j.bone.2015.05.022>
- Furuta, T., Miyaki, S., Ishitobi, H., Ogura, T., Kato, Y., Kamei, N., Miyado, K., Higashi, Y., & Ochi, M. (2016). Mesenchymal stem cell-derived exosomes promote fracture healing in a mouse model. *Stem Cells Translational Medicine*, 5(12), 1620–1630. <https://doi.org/10.5966/sctm.2015-0285>
- Gimble, J. M., Katz, A. J., & Bunnell, B. A. (2007). Adipose-derived stem cells for regenerative medicine. *Circulation Research*, 100(9), 1249–1260. <https://doi.org/10.1161/01.RES.0000265074.83288.09>
- Goh, B. C., Singhal, V., Herrera, A. J., Tomlinson, R. E., Kim, S., Faugere, M.-C., Germain-Lee, E. L., Clemens, T. L., Lee, S.-J., & Digirolamo, D. J. (2017). Activin receptor type 2A (ACVR2A) functions directly in osteoblasts as a negative regulator of bone mass. *Journal of Biological Chemistry*, 292(33), 13809–13822. <https://doi.org/10.1074/jbc.M117.782128>
- Huang, Y., Yang, Y., Wang, J., Yao, S., Yao, T., Xu, Y., Chen, Z., Yuan, P., Gao, J., Shen, S., & Ma, J. (2021). MiR-21-5p targets SKP2 to reduce osteoclastogenesis in a mouse model of osteoporosis. *Journal of Biological Chemistry*, 296, 100617. <https://doi.org/10.1016/j.jbc.2021.100617>
- Iezaki, T., Fukasawa, K., Park, G., Horie, T., Kanayama, T., Ozaki, K., Onishi, Y., Takahata, Y., Nakamura, Y., Takarada, T., Yoneda, Y., Nakamura, T., Vacher, J., & Hinoi, E. (2016). Transcriptional modulator *Irf1* regulates osteoclast differentiation through enhancing the NF-KB/NFATc1 pathway. *Molecular and Cellular Biology*, 36(19), 2451–2463. <https://doi.org/10.1128/mcb.01075-15>
- Jung, Y. J., Kim, H. K., Cho, Y., Choi, Ji S., Woo, C. H., Lee, K. S., Sul, J. H., Lee, C. M. i., Han, J., Park, J. H., Jo, D.-G., & Cho, Y. W. (2020). Cell reprogramming using extracellular vesicles from differentiating stem cells into white/beige adipocytes. *Science Advances*, 6(13), eaay6721. <https://doi.org/10.1126/sciadv.aay6721>
- Kajita, T., Ariyoshi, W., Okinaga, T., Mitsugi, S., Tominaga, K., & Nishihara, T. (2018). Mechanisms involved in enhancement of osteoclast formation by activin-A. *Journal of Cellular Biochemistry*, 119(8), 6974–6985. <https://doi.org/10.1002/jcb.26906>
- Kempen, D. H. R., Creemers, L. B., Alblas, J., Lu, L., Verbout, A. J., Yaszemski, M. J., & Dhert, W. J. A. (2010). Growth factor interactions in bone regeneration. *Tissue Engineering. Part B, Reviews*, 16(6), 551–566. <https://doi.org/10.1089/ten.teb.2010.0176>
- Khosla, S., & Hofbauer, L. C. (2017). Osteoporosis treatment: Recent developments and ongoing challenges. *Lancet Diabetes Endocrinol.*, 5(11), 898–907. [https://doi.org/10.1016/S2213-8587\(17\)30188-2](https://doi.org/10.1016/S2213-8587(17)30188-2)
- Kocan, B., Maziarz, A., Tabarkiewicz, J., Ochiya, T., & Banaś-Ząbczyk, A. (2017). Trophic activity and phenotype of adipose tissue-derived mesenchymal stem cells as a background of their regenerative potential. *Stem Cells International*, 2017, 1–13. <https://doi.org/10.1155/2017/1653254>
- Lee, S.-W., Kwak, H.-B., Lee, H.-C., Lee, S.-Ku, Kim, H.-H., & Lee, Z.-H. (2002). The anti-proliferative gene *TIS21* is involved in osteoclast differentiation. *Journal of Biochemistry and Molecular Biology*, 35(6), 609–614. <https://doi.org/10.5483/bmbrep.2002.35.6.609>
- Lener, T., Gimona, M., Aigner, L., Börger, V., Buzas, E., Camussi, G., Chaput, N., Chatterjee, D., Court, F. A., Portillo, H. A. D., O'driscoll, L., Fais, S., Falcon-Perez, J. M., Felderhoff-Mueser, U., Fraile, L., Gho, Y. S., Görgens, A., Gupta, R. C., Hendrix, A., ... Giebel, B. (2015). Applying extracellular vesicles based therapeutics in clinical trials—An ISEV position paper. *Journal of Extracellular Vesicles*, 4(1), 30087. <https://doi.org/10.3402/jev.v4.30087>
- Li, D., Liu, J., Guo, B., Liang, C., Dang, L., Lu, C., He, X., Cheung, H. Y.-S., Xu, L., Lu, C., He, B., Liu, B., Shaikh, A. B., Li, F., Wang, L., Yang, Z., Au, D. W.-T., Peng, S., Zhang, Z., ... Zhang, Ge (2016). Osteoclast-derived exosomal MiR-214-3p inhibits osteoblastic bone formation. *Nature Communications*, 7(1), 10872. <https://doi.org/10.1038/ncomms10872>
- Li, H., Yang, F., Wang, Z., Fu, Q., & Liang, A. (2015). MicroRNA-21 promotes osteogenic differentiation by targeting small mothers against decapentaplegic 7. *Molecular medicine reports*, 12(1), 1561–1567. <https://doi.org/10.3892/mmr.2015.3497>
- Li, W., Liu, Y., Zhang, P., Tang, Y., Zhou, M., Jiang, W., Zhang, X., Wu, G., & Zhou, Y. (2018). Tissue-engineered bone immobilized with human adipose stem cells-derived exosomes promotes bone regeneration. *ACS Applied Materials & Interfaces*, 10(6), 5240–5254. <https://doi.org/10.1021/acsami.7b17620>
- Lian, J. B., Stein, G. S., Van Wijnen, A. J., Stein, J. L., Hassan, M. Q., Gaur, T., & Zhang, Y. (2012). MicroRNA control of bone formation and homeostasis. *Nature Reviews Endocrinology*, 8(4), 212–227. <https://doi.org/10.1038/nrendo.2011.234>
- Lin, J. T., & Lane, J. M. (2004). Osteoporosis: A review. *Clinical Orthopaedics and Related Research*, 425, 126–134.
- Lin, W., Xu, L., Zwillingenberger, S., Gibon, E., Goodman, S. B., & Li, G. (2017). Mesenchymal stem cells homing to improve bone healing. *Journal of orthopaedics Translation*, 9, 19–27. <https://doi.org/10.1016/j.jot.2017.03.002>

- Liu, Y., & Holmes, C. (2021). Tissue regeneration capacity of extracellular vesicles isolated from bone marrow-derived and adipose-derived mesenchymal stromal/stem cells. *Frontiers Cell & developmental biology*, 9(February), 648098. <https://doi.org/10.3389/fcell.2021.648098>
- Lo, J. C., O'ryan, F. S., Gordon, N. P., Yang, J., Hui, R. L., Martin, D., Hutchinson, M., Lathon, P. V., Sanchez, G., Silver, P., Chandra, M., McCloskey, C. A., Staffa, J. A., Willy, M., Selby, J. V., & Go, A. S. (2010). Prevalence of osteonecrosis of the jaw in patients with oral bisphosphonate exposure. *Journal of Oral and Maxillofacial Surgery*, 68(2), 243–253. <https://doi.org/10.1016/j.joms.2009.03.050>
- Maqsood, M., Kang, M., Wu, X., Chen, J., Teng, L., & Qiu, L. (2020). Adult mesenchymal stem cells and their exosomes: sources, characteristics, and application in regenerative medicine. *Life Sciences*, 256, 118002. <https://doi.org/10.1016/j.lfs.2020.118002>
- Materozzi, M., Merlotti, D., Gennari, L., & Bianciardi, S. (2018). The potential role of MiRNAs as new biomarkers for osteoporosis. *International Journal Of Endocrinology*, 2018, 2342860. <https://doi.org/10.1155/2018/2342860>
- McClung, M. R. (2006). Inhibition of RANKL as a treatment for osteoporosis: preclinical and early clinical studies. *Current Osteoporosis Reports*, 4(1), 28–33. <https://doi.org/10.1007/s11914-006-0012-7>
- McClung, M. (2007). Role of RANKL inhibition in osteoporosis. *Arthritis Research & Therapy*, 9(Suppl 1), S3. <https://doi.org/10.1186/ar2167>
- Meng, F., Henson, R., Wehbe-Janek, H., Ghoshal, K., Jacob, S. T., & Patel, T. (2007). MicroRNA-21 regulates expression of the PTEN tumor suppressor gene in human hepatocellular cancer. *Gastroenterology*, 133(2), 647–658. <https://doi.org/10.1053/j.gastro.2007.05.022>
- Mizuno, A., Amizuka, N., Irie, K., Murakami, A., Fujise, N., Kanno, T., Sato, Y., Nakagawa, N., Yasuda, H., Mochizuki, S.-I., Gomibuchi, T., Yano, K., Shima, N., Washida, N., Tsuda, E., Morinaga, T., Higashio, K., & Ozawa, H. (1998). Severe osteoporosis in mice lacking osteoclastogenesis inhibitory factor/osteoprotegerin. *Biochemical and Biophysical Research Communications*, 247(3), 610–615. <https://doi.org/10.1006/bbrc.1998.8697>
- Morianos, I., Papadopoulou, G., Semitekolou, M., & Xanthou, G. (2019). Activin-A in the regulation of immunity in health and disease. *Journal of Autoimmunity*, 104(August), 102314. <https://doi.org/10.1016/j.jaut.2019.102314>
- Narayanan, R., Huang, C.-C., & Ravindran, S. (2016). Hijacking the cellular mail: Exosome mediated differentiation of mesenchymal stem cells. *Stem Cells International*, 2016, 1–11. <https://doi.org/10.1155/2016/3808674>
- Nelson, C. A., Warren, J. T., Wang, M. W.-H., Teitelbaum, S. L., & Fremont, D. H. (2012). RANKL employs distinct binding modes to engage RANK and the osteoprotegerin decoy receptor. *Structure (London, England)*, 20(11), 1971–1982. <https://doi.org/10.1016/j.str.2012.08.030>
- Ocarino, N. D. M., Boeloni, J. N., Jorgetti, V., Gomes, D. A., Goes, A. M., & Serakides, R. (2010). Intra-bone marrow injection of mesenchymal stem cells improves the femur bone mass of osteoporotic female rats. *Connective Tissue Research*, 51(6), 426–433. <https://doi.org/10.3109/03008201003597049>
- Phinney, D. G., & Pittenger, M. F. (2017). Concise review: MSC-derived exosomes for cell-free therapy. *Stem Cells*, 35(4), 851–858. <https://doi.org/10.1002/stem.2575>
- Qi, X., Zhang, J., Yuan, H., Xu, Z., Li, Q., Niu, X., Hu, B., Wang, Y., & Li, X. (2016). Exosomes secreted by human-induced pluripotent stem cell-derived mesenchymal stem cells repair critical-sized bone defects through enhanced angiogenesis and osteogenesis in osteoporotic rats. *International Journal of Biological Sciences*, 12(7), 836–849. <https://doi.org/10.7150/ijbs.14809>
- Qin, Y., Wang, L., Gao, Z., Chen, G., & Zhang, C. (2016). Bone marrow stromal/stem cell-derived extracellular vesicles regulate osteoblast activity and differentiation in vitro and promote bone regeneration in vivo. *Scientific Reports*, 6(1), 21961. <https://doi.org/10.1038/srep21961>
- Ragni, E., Perucca Orfei, C., De Luca, P., Lugano, G., Viganò, M., Colombini, A., Valli, E., Zacchetti, D., Bollati, V., & De Girolamo, L. (2019). Interaction with hyaluronan matrix and miRNA cargo as contributors for in vitro potential of mesenchymal stem cell-derived extracellular vesicles in a model of human osteoarthritic synoviocytes. *Current Stem Cell Research & Therapy*, 10(1), 109. <https://doi.org/10.1186/s13287-019-1215-z>
- Saita, Y., Ishijima, M., & Kaneko, K. (2015). Atypical femoral fractures and bisphosphonate use: Current evidence and clinical implications. *Therapeutic Advances In Chronic Disease*, 6(4), 185–193. <https://doi.org/10.1177/2040622315584114>
- Schoenmaker, T., Botman, E., Sariyildiz, M., Micha, D., Netelenbos, C., Bravenboer, N., Kelder, A., Eekhoff, E. M. W., & De Vries, T. J. (2020). Activin-A induces fewer, but larger osteoclasts from monocytes in both healthy controls and fibrodysplasia ossificans progressiva patients. *Frontiers in Endocrinology (Lausanne)*, 11(July), 1–12. <https://doi.org/10.3389/fendo.2020.00501>
- Stein, E. V., Duewer, D. L., Farkas, N., Romsos, E. L., Wang, L., & Cole, K. D. (2017). Steps to achieve quantitative measurements of MicroRNA using two step droplet digital PCR. *Plos One*, 12(11), e0188085. <https://doi.org/10.1371/journal.pone.0188085>
- Stewart, S. A. (2003). Lentivirus-delivered stable gene silencing by RNAi in primary cells. *Rna*, 9(4), 493–501. <https://doi.org/10.1261/rna.2192803>
- Su, P., Tian, Ye, Yang, C., Ma, X., Wang, X., Pei, J., & Qian, A. (2018). Mesenchymal stem cell migration during bone formation and bone diseases therapy. *International Journal of Molecular Sciences*, 19(8), 2343. <https://doi.org/10.3390/ijms19082343>
- Tobeiha, M., Moghadasian, M. H., Amin, N., & Jafarnejad, S. (2020). RANKL/RANK/OPG pathway: A mechanism involved in exercise-induced bone remodeling. *BioMed research international*, 2020, 6910312. <https://doi.org/10.1155/2020/6910312>
- Tolar, J., Nauta, A. J., Osborn, M. J., Panoskaltsis Mortari, A., Mcclumurry, R. T., Bell, S., Xia, L., Zhou, N., Riddle, M., Schroeder, T. M., Westendorf, J. J., Mcivor, R. S., Hogendoorn, P. C. W., Szuhai, K., Oseth, L., Hirsch, B., Yant, S. R., Kay, M. A., Peister, A., & ... Blazar, B. R. (2007). Sarcoma derived from cultured mesenchymal stem cells. *Stem Cells*, 25(2), 371–379. <https://doi.org/10.1634/stemcells.2005-0620>
- Vlassov, A. V., Magdaleno, S., Setterquist, R., & Conrad, R. (2012). Exosomes: Current knowledge of their composition, biological functions, and diagnostic and therapeutic potentials. *Biochimica et Biophysica Acta*, 1820(7), 940–948. <https://doi.org/10.1016/j.bbagen.2012.03.017>
- Wang, L., Li, Yi, Chen, J., Gautam, S. C., Zhang, Z., Lu, M., & Chopp, M. (2002). Ischemic cerebral tissue and MCP-1 enhance rat bone marrow stromal cell migration in interface culture. *Experimental Hematology*, 30(7), 831–836. [https://doi.org/10.1016/S0301-472X\(02\)00829-9](https://doi.org/10.1016/S0301-472X(02)00829-9)
- Wang, Z., Goh, J., De, S. D., Ge, Z., Ouyang, H., Chong, J. S. W., Low, S. L., & Lee, E. H. (2006). Efficacy of bone marrow-derived stem cells in strengthening osteoporotic bone in a rabbit model. *Tissue Engineering*, 12(7), 1753–1761. <https://doi.org/10.1089/ten.2006.12.1753>
- Woo, C. H., Kim, H. K., Jung, G. Y., Jung, Y. J., Lee, K. S., Yun, Ye E., Han, J., Lee, J., Kim, W. S., Choi, Ji S., Yang, S., Park, J. H., Jo, D. - G., & Cho, Y. W. (2020). Small extracellular vesicles from human adipose-derived stem cells attenuate cartilage degeneration. *Journal of Extracellular Vesicles*, 9(1). <https://doi.org/10.1080/20013078.2020.1735249>
- Xu, Ji-F., Yang, G.-H., Pan, X.-H., Zhang, S.-J., Zhao, C., Qiu, B.-S., Gu, H.-F., Hong, J.-F., Cao, Li, Chen, Yu, Xia, B., Bi, Q., & Wang, Ya-P. (2014). Altered microRNA expression profile in exosomes during osteogenic differentiation of human bone marrow-derived mesenchymal stem cells. *Plos One*, 9(12), e114627. <https://doi.org/10.1371/journal.pone.0114627>
- Yao, W., Guan, M., Jia, J., Dai, W., Lay, Y.-A. E., Amugongo, S., Liu, R., Olivos, D., Saunders, M., Lam, K. S., Nolta, J., Olvera, D., Ritchie, R. O., & Lane, N. E. (2013). Reversing bone loss by directing mesenchymal stem cells to bone. *Stem Cells*, 31(9), 2003–2014. <https://doi.org/10.1002/stem.1461>
- Yeo, R. W. Y., Lai, R. C., Zhang, B., Tan, S. S., Yin, Y., Teh, B. J., & Lim, S. K. (2013). Mesenchymal stem cell: An efficient mass producer of exosomes for drug delivery. *Advanced Drug Delivery Reviews*, 65(3), 336–341. <https://doi.org/10.1016/j.addr.2012.07.001>
- Zhang, J., Liu, X., Li, H., Chen, C., Hu, B., Niu, X., Li, Q., Zhao, B., Xie, Z., & Wang, Y. (2016). Exosomes/tricalcium phosphate combination scaffolds can enhance bone regeneration by activating the PI3K/Akt signaling pathway. *Current Stem Cell Research & Therapy*, 7(1), 136. <https://doi.org/10.1186/s13287-016-0391-3>

Zhao, R., Li, Y., Lin, Z., Wan, J., Xu, C., Zeng, Y., & Zhu, Y. (2016). MiR-199b-5p Modulates BMSC osteogenesis via suppressing GSK-3 β / β -catenin signaling pathway. *Biochemical and Biophysical Research Communications*, 477(4), 749–754. <https://doi.org/10.1016/j.bbrc.2016.06.130>

SUPPORTING INFORMATION

Additional supporting information may be found in the online version of the article at the publisher's website.

How to cite this article: Lee, K. S., Lee, J., Kim, H. K., Yeom, S Ho, Woo, C. H., Jung, Y. J., Yun, Ye E, Park, So Y, Han, J., Kim, E., Sul, J. H., Jung, J. M., Park, J. H., Choi, Ji S, Cho, Y. W., & Jo, D.-G. (2021). Extracellular vesicles from adipose tissue-derived stem cells alleviate osteoporosis through osteoprotegerin and *miR-21-5p*. *Journal of Extracellular Vesicles*, 10, e12152. <https://doi.org/10.1002/jev2.12152>